Send Orders for Reprints to reprints@benthamscience.ae

The Open Construction and Building Technology Journal, 2018, *11*, 3-00

The Open Construction and Building Technology Journal

Content list available at: www.benthamopen.com/TOBCTJ/

DOI: 10.2174/1874836801812010197

RESEARCH ARTICLE

Thermal Performance of Resource-Efficient Geopolymeric Mortars Containing Phase Change Materials

M. Kheradmand[1], F. Pacheco-Torgal[1,2,*] and M. Azenha[3]

[1]*C-TAC Research Centre, University of Minho, Guimarães, Portugal*
[2]*SHRC, University of Sungkyunkwan, Suwon, Republic of Korea*
[3]*ISISE, University of Minho, Guimarães, Portugal*

Received: February 16, 2018 Revised: June 06, 2018 Accepted: June 11, 2018

Abstract:

Background:

Energy efficiency is not only the most cost effective way to reduce emissions but also a way to improve competitiveness and create employment. Geopolymeric mortars containing phase change materials-PCMs have a twofold positive impact concerning eco-efficiency. On one hand, the mortars are based on industrial waste contributing for resource efficiency. And on the other hand, PCM based mortars have the capacity to enhance the thermal performance of the buildings.

Object:

This paper reports experimental results on the thermal performance of geopolymeric mortars containing different percentages of phase-change materials-PCMs.

Method:

Five groups of alkali-activated based mortars with different PCM percentages were produced and placed on a panel within a small scale prototype for thermal performance testing.

Results:

The results show that the thermal conductivity of the mortars decreased with the increase in the percentage of the PCM.

Conclusion:

Thermal performance of the PCM based mortars allowed for a stronger attenuation of the temperature amplitudes. Both for heating and cooling loads.

Keywords: Energy efficiency, Waste reuse, Fly ash, Geopolymers, PCMs, Thermal performance.

1. INTRODUCTION

Energy production based on non-renewable fossil fuels is mainly responsible for global greenhouse-gas emissions (GHGs) [1]. In EU, the building sector is the largest energy user responsible for about 40% of the total final energy consumption. According to the Energy Road Map 2050 [2], higher energy efficiency in new and existing buildings is key for the transformation of the EU's energy system. Energy efficiency is not only the most cost effective way to reduce emissions but also a way to improve competitiveness and create employment [3]. The European Energy Performance of Buildings Directive 2002/91/EC (EPBD) has been recast in the form of the 2010/31/ EU by the

* Address correspondence to this author at the C-TAC Research Centre, University of Minho, Campus de Azurem, Guimarães, Portugal; Tel: 253-510200; E-mail: torgal@civil.uminho.pt

European Parliament on 19 May 2010 [4].One of the new aspects of the EPBD is the introduction of the concept of nearly zero-energy (public) building (NZEB) by the end of 2018 (2020 for private buildings). This very ambitious target would be more easily fulfilled if high thermal performance materials like PCMs are to be used [5]. PCMs use chemical bonds to store or release heat hence reducing energy consumption. Depending on the air temperature, PCMs can change from solid to liquid or liquid to solid, absorbing or releasing heat during the process. Therefore, they can absorb heat inside buildings avoiding excessive heating and reducing cooling needs. There are basically three main groups of PCMs: (i) organic; (ii) inorganic; and (iii) eutectic. In the scope of construction materials, the organic group is more popular due to its cost-effectiveness, desirable melting temperature range, stability and good durability upon repeated heating/cooling cycles [6]. PCMs themselves (*e.g.* paraffins) can be directly incorporated into cement-based materials simply by mixing them as a part of composite mixture. However, after several temperature cycles, the paraffins may start leaking [7]. In order to solve the leakage problem, encapsulation techniques have been be applied to paraffins, with successful applications of both microencapsulated and macrcoencapsulated PCMs [8]. Encapsulation techniques lead however to an added cost in PCM based mortars. According to the literature survey, macro encapsulated PCMs present limitations in heat transfer because of the hampering effect of the PCM in the surface region of the macrocapsule that strongly hinders temperature variations of the core of the macrocapsule. Several studies have investigated the use of microencapsulated PCM in different applications [9 - 12]. Also the flagship initiative "A resource-efficient Europe" highlights the importance of increasing resource efficiency as key to bring major economic opportunities, improve productivity, drive down costs and boost competitiveness. According to the Roadmap to a Resource Efficient Europe "*By 2020, waste is managed as a resource"* [13]. This is a very important goal in the European context of a circular economy and zero waste target [14]. Thus materials that have the ability for the reuse of several types of wastes such as geopolymeric will merit a special attention. Geopolymers are low calcium binder materials produced through the reaction of an aluminosilicate with an alkaline activator, leading to the formation an amorphous aluminosilicate gel and secondary nano crystalline zeolite-like structures [15]. Research works carried out so far in the development of these materials showed that much has already been investigated, especially concerning the ability for waste reuse [16 - 21]. Some wastes like fly ash deserve an especial attention because they are generated in high amount and have a very low reuse rate [22]. In this context, this paper reports experimental results on the thermal performance of geopolymeric fly ash mortars containing PCMs.

2. EXPERIMENTAL

The study includes the characterization of the geopolymeric mortars, density, thermal conductivity and thermal behavior by DSC (differential scanning calorimetry). The microencapsulated PCMs were directly incorporated into the mortar and applied as disc shape in the center of extruded polystyrene (XPS) panel that was placed within a hollow horizontal tunnel using walls made of XPS. This pilot prototype was placed inside a climatic chamber initialized at specific temperature ranges.

2.1. Materials and Formulations

The raw materials used for the preparation of the geopolymeric mortars were fly ash, calcium hydroxide, sand, sodium silicate, sodium hydroxide, PCMs and superplastisizer. Solid sodium hydroxide supplied by ERCROS, S.A., was used to prepare the 12M NaOH solution. Distilled water was used to dissolve the sodium hydroxide flakes to avoid the effect of unknown contaminants in the mixing water. The NaOH mix was made one day prior to use in order to produce a homogenous solution. The chemical composition of the sodium hydroxide was 25% Na_2O and 75% H_2O. The sodium silicate liquid was supplied by MARCANDE, Portugal. The chemical composition of the sodium silicate was of 13.5% Na_2O, 58.7% SiO_2 and 45.2% H_2O. The fly ash was obtained from The PEGO Thermal Power Plant in Portugal and it was classified as class F according to ASTM-C618 [23] standard. Fig. (**1**) shows an SEM image of fly ash. The smallest fly ash particles were around 2μm in diameter and the largest reached approximately 59 μm. The chemical composition of the fly ash is presented in Table **1**. One type of organic Microencapsulated PCM was used, type BSF26 with a melting temperature of 26 ºC. The properties of the PCM are presented in Table **2**. The technical specifications of the PCMs, report encapsulated spherical paraffin particles of around 18 μm. SEM imaging of PCM particles indicated a large variation of the particle size. The smallest PCM particles were around 3 μm in diameter and the largest reached approximately 26 μm (Fig. **2**).The calcium hydroxide was provided by LUSICAL H100 and contains more than 99% CaO. The sand was supplied by MIBAL, Minas de Barqueiros, S.A. Portugal. Prior to its use it was sieved in order to remove dust particles. The sieves used in this operation had a 4.75mm and a 0.6mm mesh size. The superplastisizer was supplied by BASF. It's a polyacrylate from Acronal series, with a density of 1050 $kg.m^3$.

Table 1. Major oxides in fly ash.

Material	Oxides (wt.%)							
	SiO_2	Al_2O_3	Fe_2O_3	CaO	MgO	Na_2O	K_2O	TiO_2
Fly Ash	60.81	22.68	7.64	1.01	2.24	1.45	2.7	1.46
LOI 3% 2,42 g/cm^3 Blaine surface area 3848 g/cm^2								

Table 2. Properties of PCMs [31].

PCM type	Operating temperature ranges (ºC)	Latent heat of fusion (J/g)	Melting point (ºC)	Apparent density at solid state (kg/m^3)	Particle size distribution range (µm)
BSF26	10-30	110	26	350	5-90

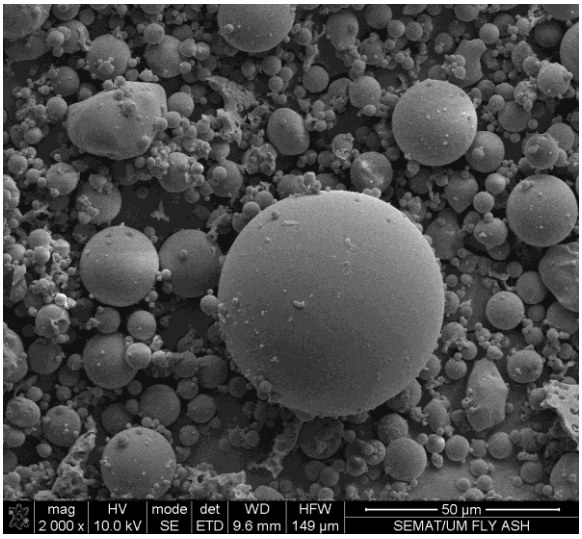

Fig. (1). SEM image of (a) fly ash

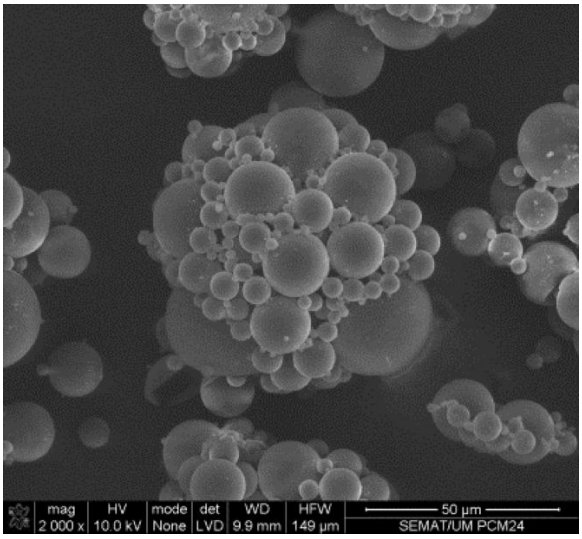

Fig. (2). SEM image of microencapsulated PCM (BSF26)

2.1.1. Mortars Design and Production

The mix design is shown in Table **3**. A sodium hydroxide solution (12M) was mixed with sodium silicate to dissolve the silica and alumina of the fly ash particles, resulting in a homogenized gel lasting 1 min; next, all the solid

materials were mixed by using standard mixer operating at the following speed I (65rpm) for 3 min. After the addition of the alkaline activator, the mixer was operated during 1min with speed I (65rpm) and plus another 1 min with speed II (90rpm). Afterward, the mixture was placed into moulds. The specimens were kept at room conditions with temperature around 25 ˚C and relative humidity of 65%RH. After 4h the hardened specimens were demoulded and sealed with plastic wrap and then left in the same room till the testing age.

Table 3. Mix proportion for the AACB mortars.

Formulations	Group Name	Materials (kg/m^3)*								
		PC	FA	CH	Sand	SS	SH	SP	WT	PCM
90FA_10CH_12M_2.5S/H_0.8A/B	A	0	438.5	48.7	1461.5	278	111.7	0	0	0.0
90FA_10PC_12M_2.5S/H_0.8A/B	E	49	441.5	0	1471.3	280	112.5	0	0	0.0
90FA_10CH_12M_2.5S/H_0.7A/B_1.0SP	B	0	448.4	49.9	1495.6	249.1	99.7	5.5	0	0.0
90FA_10CH_12M_2.0S/H_0.7A/B_1.0SP	C	0	445	49.5	1483.4	230.8	115.4	5.5	0	0.0
90FA_10CH_12M_1.5S/H_0.7A/B_1.0SP	D	0	439.8	48.9	1465.8	206.3	137.9	5.4	0	0.0
90FA_10CH_10PCM_12M_2.5S/H_0.8A/B	A	0.0	421	46.8	1262.8	266.9	107.2	0.0	0.0	32.3
90FA_10PC_10PCM_12M_2.5S/H_0.8A/B	E	47.1	423.6	0.0	1270.8	268.6	107.9	0.0	0.0	32.5
90FA_10CH_10PCM_12M_2.5S/H_0.7A/B_1.5SP	B	0.0	428.9	47.7	1286.8	238.3	95.3	7.9	0.0	32.9
90FA_10CH_10PCM_12M_2.0S/H_0.7A/B_1.5SP	C	0.0	425.8	47.3	1277.5	220.8	110.4	7.9	0.0	32.6
90FA_10CH_10PCM_12M_1.5S/H_0.7A/B_1.5SP	D	0.0	421	46.8	1263.1	197.5	132	7.8	0.0	32.3
90FA_10CH_20PCM_12M_2.5S/H_0.8A/B	A	0.0	422.3	46.9	1125.9	267.7	107.6	0.0	0.0	50
90FA_10PC_20PCM_12M_2.5S/H_0.8A/B	E	47.2	424.9	0.0	1133.2	269.5	108.3	0.0	0.0	50.4
90FA_10CH_20PCM_12M_2.5S/H_0.7A/B_1.5SP	B	0.0	430.3	47.8	1147.5	239	95.6	7.8	0.0	51
90FA_10CH_20PCM_12M_2.0S/H_0.7A/B_1.5SP	C	0.0	427.2	47.5	1139.2	221.5	110.8	7.9	0.0	50.6
90FA_10CH_20PCM_12M_1.5S/H_0.7A/B_1.5SP	D	0.0	422.3	46.9	1126.2	198.1	132.4	7.8	0.0	50
90FA_10CH_30PCM_12M_2.5S/H_0.8A/B	A	0.0	393.1	43.7	917.3	249.3	100.2	0.0	0.0	87.4
90FA_10PC_30PCM_12M_2.5S/H_0.8A/B	E	43.9	395.5	0.0	922.9	250.8	100.8	0.0	0.0	87.9
90FA_10CH_30PCM_12M_2.5S/H_0.7A/B_1.5SP	B	0.0	400.1	44.5	933.6	222.3	88.9	7.4	0.0	89
90FA_10CH_30PCM_12M_2.0S/H_0.7A/B_1.5SP_3.0W	C	0.0	391.5	43.5	913.5	203	101.5	7.2	14.5	87.1
90FA_10CH_30PCM_12M_1.5S/H_0.7A/B_1.5SP_3.0W	D	0.0	387.4	43	904	181.7	121.5	7.2	14.3	86.2

*PC: Portland cement; FA: fly ash; CH: calcium hydroxide; SS: sodium silicate; SH: sodium hydroxide; SP: superplastisizer; PCM: phase change materials; and WT: water.

2.1.2. Testing

2.1.2.1. Density

For density assessment, three specimens were considered for each type of mortar. The test was designed according to EN1015:10 [24]. Firstly, the specimens were casted into cubic moulds (with dimensions of 50 mm×50 mm×50 mm). Then the specimens were kept sealed with a plastic sheet at laboratory environment (25 ºC) for about 24h. Afterward, the specimens were submerged at 20 ± 1°C for 7 days. Then, the specimens were dried at 70 °C until constant mass was reached. The dimensions of the specimens were measured using a digital caliper with a precision of 0.02 mm, and their weights were measured using an analytical balance with a precision of 0.001 g.

2.1.2.2. Thermal Conductivity

The thermal conductivities were determined with four representative measurements for each mortar formulation, using a steady state heat flow meter apparatus (ALAMBETA, Model Sensora), according to ISO8301:1991 [25]. This device has an accuracy of 0.005 W/mK .Mortars were casted into cylinder moulds with a diameter of 10 cm and length of 1 cm. Then, the specimens were kept sealed and cured for 28 days at laboratory conditions on temperature of 25 ºC. The thermal conductivity of the specimen was calculated based on heat conduction heat transfer theory according to [26].

2.1.2.3. Thermal Energy Storage

In order to provide information about the specific enthalpies of the mortars, it is relevant to submit the specimens into the DSC testing (Model NETZSCH 200 F3 Maia) and measure the corresponding heat fluxes at controlled temperature. This device has an accuracy of ±0.2 ˚C.The specific heat and the specific enthalpy were determined

following the recommendations adopted in [27]. All the specimens were tested within aluminium crucibles with volume of 40µL under nitrogen (N_2) atmosphere with a flow of 50mL/min. The specimens were weighted using an analytical balance (model Perkin Elmer AD-4) with an accuracy of ±0.01 mg. Each specimen was sealed in the pan by using an encapsulating press. An empty aluminium crucible was considered as a reference in all measurements. A heating/cooling rate of 5 ºC/min was considered for all experiments [28].

2.1.2.4. Design and Fabrication of the Pilot Prototypes

A total of 20 panels with dimensions of 30 cm×30 cm×3 cm were built. The mortar specimens with a diameter of 10 cm and thickness of 3 cm were placed at the geometrical center of the panels made of extruded polystyrene (XPS). Each panel was placed inside the hollow pilot prototype whose walls were made of XPS. The cross-section schematic diagram of prototype has outer dimensions of 60 cm×36 cm×36 cm (Fig. **3**). The prototype was equipped with a heater in order to produce heat through the prototype. The heater system had dimensions of 25 cm×13 cm×22.5 cm, with a power rating of 1000W and was placed on the left side of the prototype. In each experiment, the control of the heating system was set at ON mode to produce the heat for 30 minutes and then OFF mode for 30 minutes. With regard to temperature monitoring, thermocouples tyke K, were positioned at two points at the interior ambient of the prototype, here termed as "X". The two thermocouples were placed in the air ambient of the prototype: one on the left side to measure imposed temperature and another on the right side to measure interior air temperature. The thermocouples were connected to a data acquisition system (AGILENT 34970A) with a rate of one measuring per ten seconds during the whole period of testing. The prototype was placed inside a climatic chamber room with a constant temperature of 18 ºC and a relative humidity of 60% in order to ensure an initializing of the test setup at a temperature below the phase change transition of the PCM. A total of twenty experiments were conducted submitting the prototype to the environmental conditions, with each experiment lasting 60 minutes (a heating/cooling cycle).

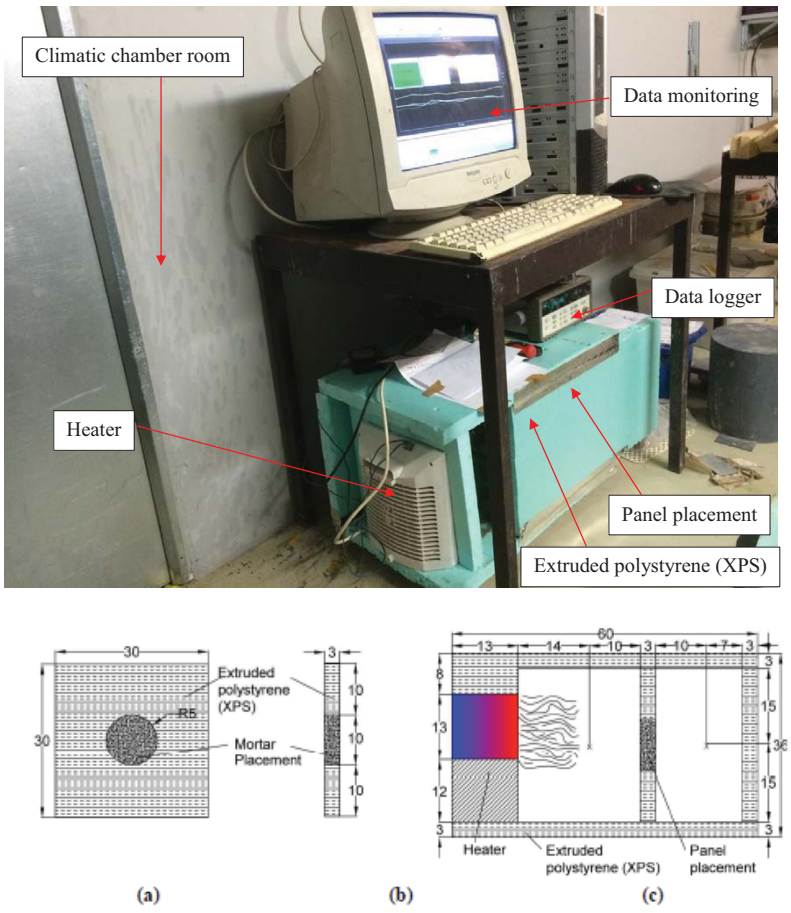

Fig. (3). Above: Photo of the prototype Below: Schematic representation of pilot prototype: (a) front view of the panel; (b) lateral view of the panel; (c) cross section of the test setup equipped with e heater together with placement of the panel inside the pilot prototype. Units: [cm].

3. RESULTS AND DISCUSSION

3.1. Characterization of materials

3.1.1. Density

The results of density can be found in Table **4**. Overall, it can be said that the percentage of PCM content is proportional to the densities of geopolymer mortars. The use of PCM with low density made the mortar mixture slightly lighter with lower density. Regarding the density difference between mortars termed as group A to E with different mass fraction of PCM, it is interesting to note that the density of mortar with incorporation of 10%PCM, 20%PCM and 30%PCM in group A is approximately 86%, 85% and 84% to that of reference mixture (mortar without PCM) in group A. Similar trends have been observed for different groups. Fig. (**4**) shows a linear correlation between density and PCM percentage. However, it is less pronounced for the mortars in groups of B, C and D due to the utilization of additives PC and CH in the mixtures.. The reason may be the lower density of PCM when compared to the density of sand.

Table 4. Density of AACB mortars.

Formulations	Group name	Density (kg/m^3)	Thermal conductivity (W/m. K)
90FA_10CH_12M_2.5S/H_0.8A/B	A	1747	0.77
90FA_10CH_10PCM_12M_2.5S/H_0.8A/B	A	1508	0.70
90FA_10CH_20PCM_12M_2.5S/H_0.8A/B	A	1496	0.69
90FA_10CH_30PCM_12M_2.5S/H_0.8A/B	A	1483	0.44
90FA_10CH_12M_2.5S/H_0.7A/B_1.0SP	B	1775	0.52
90FA_10CH_10PCM_12M_2.5S/H_0.7A/B_1.5SP	B	1578	0.47
90FA_10CH_20PCM_12M_2.5S/H_0.7A/B_1.5SP	B	1350	0.44
90FA_10CH_30PCM_12M_2.5S/H_0.7A/B_1.5SP	B	1688	0.42
90FA_10CH_12M_2.0S/H_0.7A/B_1.0SP	C	1733	0.94
90FA_10CH_10PCM_12M_2.0S/H_0.7A/B_1.5SP	C	1617	0.90
90FA_10CH_20PCM_12M_2.0S/H_0.7A/B_1.5SP	C	1541	0.77
90FA_10CH_30PCM_12M_2.0S/H_0.7A/B_1.5SP_3.0W	C	1685	0.35
90FA_10CH_12M_1.5S/H_0.7A/B_1.0SP	D	1724	0.71
90FA_10CH_10PCM_12M_1.5S/H_0.7A/B_1.5SP	D	1629	0.65
90FA_10CH_20PCM_12M_1.5S/H_0.7A/B_1.5SP	D	1528	0.59
90FA_10CH_30PCM_12M_1.5S/H_0.7A/B_1.5SP_3.0W	D	1677	0.37
90FA_10PC_12M_2.5S/H_0.8A/B	E	1801	0.91
90FA_10PC_10PCM_12M_2.5S/H_0.8A/B	E	1636	0.80
90FA_10PC_20PCM_12M_2.5S/H_0.8A/B	E	1564	0.75
90FA_10PC_30PCM_12M_2.5S/H_0.8A/B	E	1452	0.52

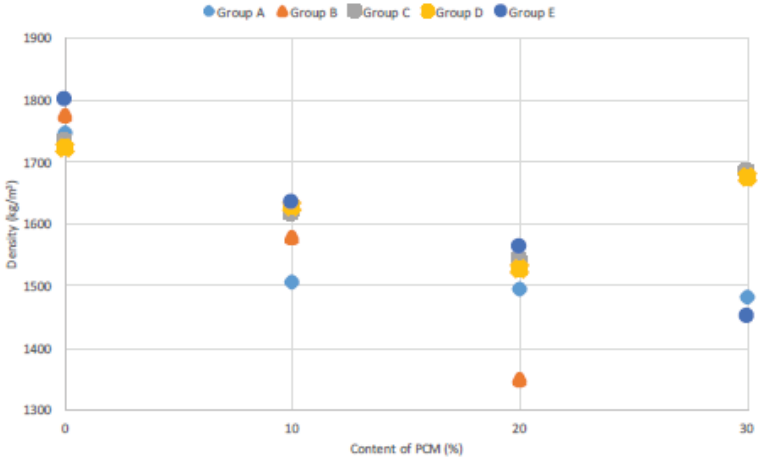

Fig. (4). Density versus PCM content for AACB mortars

3.1.2. Thermal Conductivity

Table **5**shows the thermal conductivity results. They show that the addition of microencapsulated PCM decreases the thermal conductivity of the mortars. Mortars without PCM in the groups A to E have thermal conductivities of 0.77, 0.52, 0.94, 0.71 and 0.91, respectively. Fig. (**5**) shows that the addition of 10% PCM into the mortars in group A to E leads to a reduction of thermal conductivities approximately 5% to 12%, when compared with the mortars without PCM. When a PCM percentage of 20% was used (mortars in group A to E) reductions of approximately 11% to 20% in the thermal conductivities were observed. The reductions can be as higher as 60% for mortars with a PCM percentage of 30%. These findings are in the line with the previous studies on PCM mortars [29, 30].

Table 5. Thermal conductivity of AACB mortars.

Formulations	Group name	Thermal conductivity (W/m. K)
90FA_10CH_12M_2.5S/H_0.8A/B	A	0.77
90FA_10CH_10PCM_12M_2.5S/H_0.8A/B	A	0.70
90FA_10CH_20PCM_12M_2.5S/H_0.8A/B	A	0.69
90FA_10CH_30PCM_12M_2.5S/H_0.8A/B	A	0.44
90FA_10CH_12M_2.5S/H_0.7A/B_1.0SP	B	0.52
90FA_10CH_10PCM_12M_2.5S/H_0.7A/B_1.5SP	B	0.47
90FA_10CH_20PCM_12M_2.5S/H_0.7A/B_1.5SP	B	0.44
90FA_10CH_30PCM_12M_2.5S/H_0.7A/B_1.5SP	B	0.42
90FA_10CH_12M_2.0S/H_0.7A/B_1.0SP	C	0.94
90FA_10CH_10PCM_12M_2.0S/H_0.7A/B_1.5SP	C	0.90
90FA_10CH_20PCM_12M_2.0S/H_0.7A/B_1.5SP	C	0.77
90FA_10CH_30PCM_12M_2.0S/H_0.7A/B_1.5SP_3.0W	C	0.35
90FA_10CH_12M_1.5S/H_0.7A/B_1.0SP	D	0.71
90FA_10CH_10PCM_12M_1.5S/H_0.7A/B_1.5SP	D	0.65
90FA_10CH_20PCM_12M_1.5S/H_0.7A/B_1.5SP	D	0.59
90FA_10CH_30PCM_12M_1.5S/H_0.7A/B_1.5SP_3.0W	D	0.37
90FA_10PC_12M_2.5S/H_0.8A/B	E	0.91
90FA_10PC_10PCM_12M_2.5S/H_0.8A/B	E	0.80
90FA_10PC_20PCM_12M_2.5S/H_0.8A/B	E	0.75
90FA_10PC_30PCM_12M_2.5S/H_0.8A/B	E	0.52

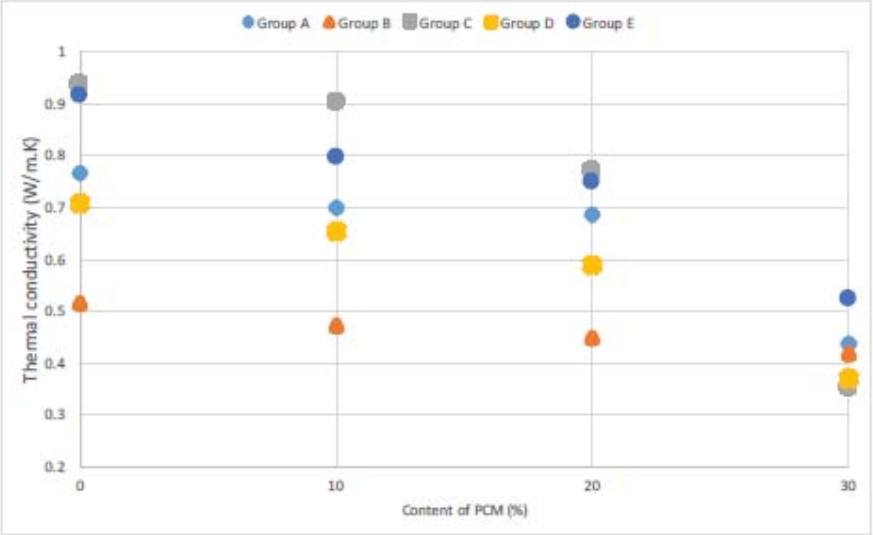

Fig. (5). Thermal conductivity versus PCM contents for AACB mortars.

3.1.3. Thermal Energy Storage

Table **6** shows the Weights of specimens used in DSC test. The steps for the test procedure were as follows: (i) initial isothermal period at 5 ºC for 5 min; (ii) dynamic heating up to 40 ºC with the rate of 5 ºC/min; (iii) stabilization at 40 ºC for 5 min; (iv) dynamic cooling to 5 ºC with the rate of 5 ºC/min. It should be mentioned that, the phase change and temperature were obtained from the DSC heat fluxes signal response by integration. The peak temperatures of heating/cooling cycle have been considered as the representative temperature of a phase change transition. The onset and end temperature for each phase change were determined according to the recommendation of the EN ISO 11357-1 [31]. Fig. (**6**) shows the DSC results for pure microencapsulated PCM. The heating process revealed a melting peak temperature coinciding with the reference value indicated by the supplier, with maximum deviation reaching 0.57 °C. The measured specific enthalpies for the pure microencapsulated PCM were lower than that reported by the supplier by 15% and 5% for heating and cooling, respectively. Furthermore, the difference between the peak temperatures of heating and cooling processes was of 7.5 K. This is coherent with the reports of hysteretic behaviour of the phase change materials [32].The DSC curves for testing of mortars in group A to E at heating/cooling rate of 5 °C/min are shown in Fig. (**7**). The peak temperatures in the thermograms of the heating processes are consistently being increased from ≈25 °C to ≈26 °C as the PCM percentage increases. Conversely, in the cooling processes (in Figs. **7a-e**), the peak temperature decreases (from ≈20.5 °C to ≈22 °C) with increased PCM percentage. The results suggested that the PCM peak temperature shifts in the direction of the imposed flux, thus showing higher peaks for mortars with high PCM percentage. This trend has also been reported by others [27, 33] and it can be explained by the increase in specific heat capacity. The representation of peak temperatures and the percentage of PCM in the mortars was made with two dashed lines that showed a clear linear relationship between them for both heating and cooling processes. The distance between phase change experienced from Δ≈1.5 K to Δ≈2.1 K which depends on the sample and on the internal thermal gradients, tends to lag or raise heat exchange from DSC test explaining the observed differences. In the tested PCM mortar samples, the phase change melting/freezing temperatures were coherent with that of the pure microencapsulated PCM. Overall differences between heating/cooling peaks in the thermograms for different mortars were observed to be smaller as the weight percentage of PCM decreased, being that such hysteretic behaviour is observed for all tested mortars with PCM. An example of such a case for the mortars at group A is presented in Fig. (**8**), where significant shifts are generally observed. It should be noted that the DSC thermograms have been zoomed to their peaks in order to facilitate the observation of the hysteretic behaviour. The difference between heating/cooling peaks (here termed as "D") was 3.5 K, 4 K, and 5 K for the mortars in group A with 10% PCM, 20% PCM and 30% PCM, respectively, and compared with the case with 100% PCM with the highest hysteretic behaviour of D≈7.5 K. It is worth noticing that when the purpose of DSC testing is to assist numerical simulation of PCM performance in building façade, it becomes apparent that the low heating/cooling rate is the one that mostly resembles real scenarios of daily temperature variation. It should be mentioned that the specific enthalpy of the PCM mortars for each phase transition is almost independent of the heating/cooling rate. Moreover, the impact of the heating/cooling rate depends on the hysteretic behaviour of the thermal response of mortars with PCM, in which, lower heating/cooling rate exhibits minimum to no apparent hysteresis. Figs. (**9** and **10**) show the volumetric heat capacity calculations and thermal inertia. These figures solely plot the results for mortars at group A upon heating process. The volumetric heat capacity (C_{pv}) of the materials is calculated by multiplying the density and specific heat capacity according to:

Table 6. Weight of specimen prepared for DSC testing.

Formulations	Group name	Weight of specimen for DSC testing (mg)
90FA_10CH_12M_2.5S/H_0.8A/B	A	19
90FA_10CH_10PCM_12M_2.5S/H_0.8A/B	A	18.09
90FA_10CH_20PCM_12M_2.5S/H_0.8A/B	A	19.1
90FA_10CH_30PCM_12M_2.5S/H_0.8A/B	A	18.3
90FA_10CH_12M_2.5S/H_0.7A/B_1.0SP	B	18.4
90FA_10CH_10PCM_12M_2.5S/H_0.7A/B_1.5SP	B	19.09
90FA_10CH_20PCM_12M_2.5S/H_0.7A/B_1.5SP	B	19.62
90FA_10CH_30PCM_12M_2.5S/H_0.7A/B_1.5SP	B	19.84
90FA_10CH_12M_2.0S/H_0.7A/B_1.0SP	C	18.62
90FA_10CH_10PCM_12M_2.0S/H_0.7A/B_1.5SP	C	19.43
90FA_10CH_20PCM_12M_2.0S/H_0.7A/B_1.5SP	C	18.18
90FA_10CH_30PCM_12M_2.0S/H_0.7A/B_1.5SP_3.0W	C	19.42

(Table 6) contd.....

Formulations	Group name	Weight of specimen for DSC testing (mg)
90FA_10CH_12M_1.5S/H_0.7A/B_1.0SP	D	19.39
90FA_10CH_10PCM_12M_1.5S/H_0.7A/B_1.5SP	D	17.71
90FA_10CH_20PCM_12M_1.5S/H_0.7A/B_1.5SP	D	18.54
90FA_10CH_30PCM_12M_1.5S/H_0.7A/B_1.5SP_3.0W	D	17.79
90FA_10PC_12M_2.5S/H_0.8A/B	E	17.5
90FA_10PC_10PCM_12M_2.5S/H_0.8A/B	E	19.42
90FA_10PC_20PCM_12M_2.5S/H_0.8A/B	E	17.95
90FA_10PC_30PCM_12M_2.5S/H_0.8A/B	E	15.4
Pure microencapsulated PCM (with melting temperature of 26ºC)	-	10.64

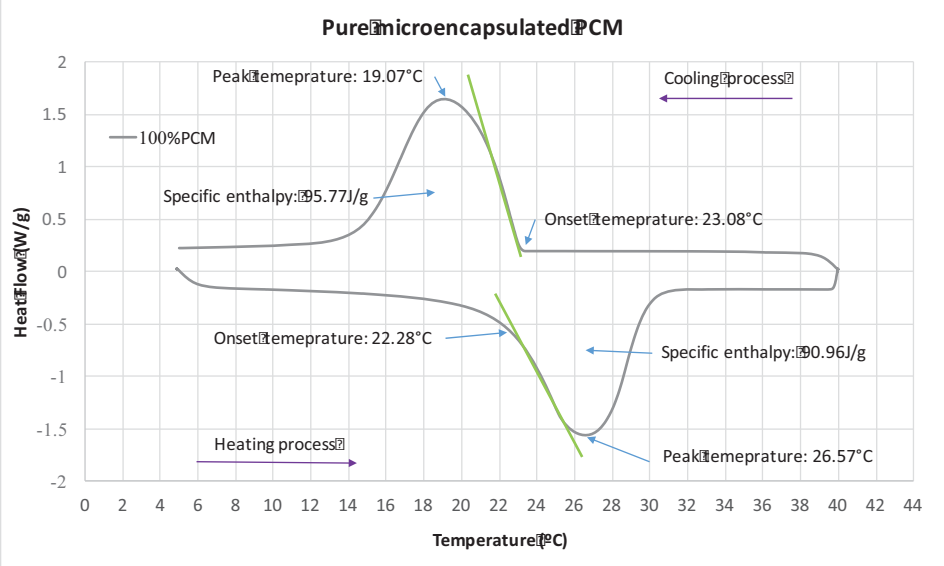

Fig. (6). DSC curve of pure microencapsulated PCM with melting temperature of 26°C upon a heating and a cooling cycle with rate of 5°C/min.

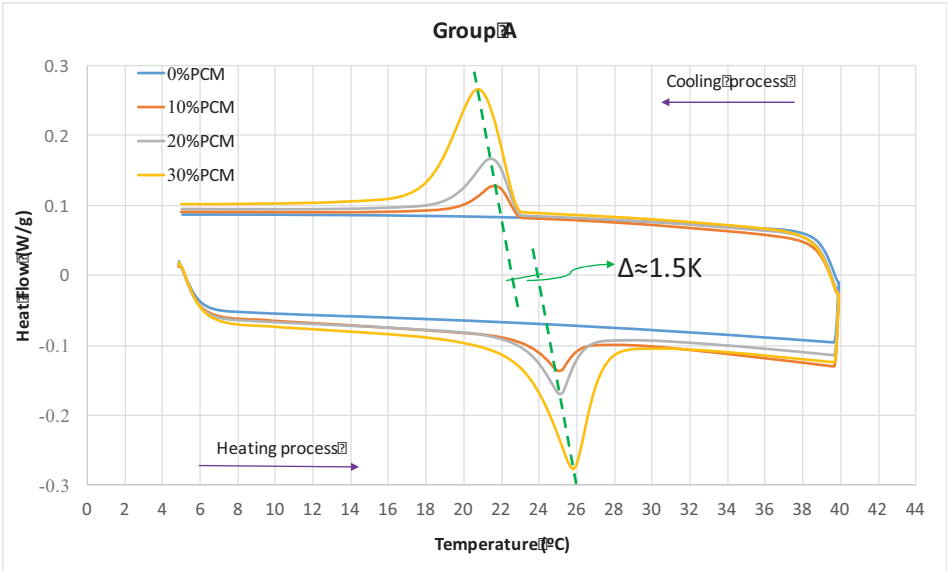

(a)

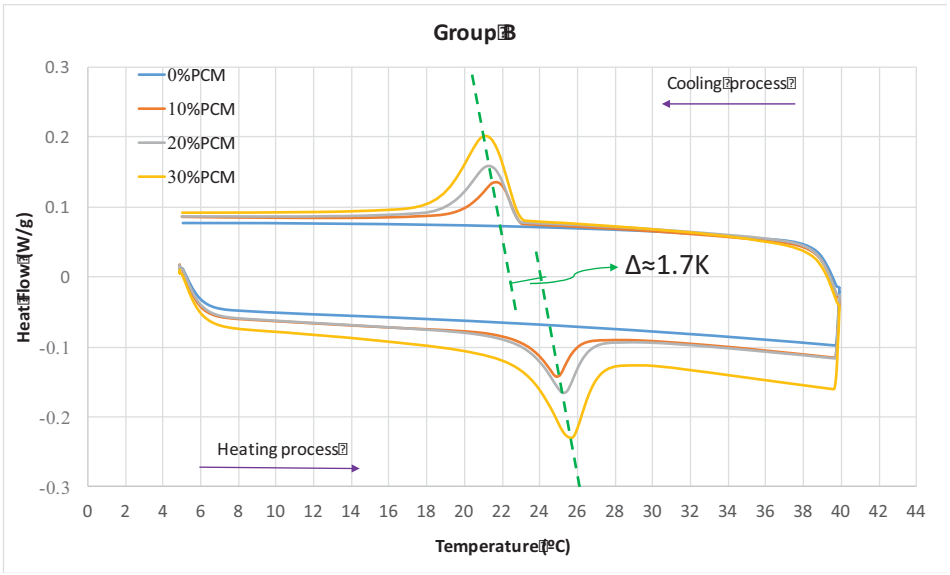
Group B
0%PCM
10%PCM
20%PCM
30%PCM
Cooling process
Δ≈1.7K
Heating process
Heat Flow (W/g)
Temperature (°C)

(b)

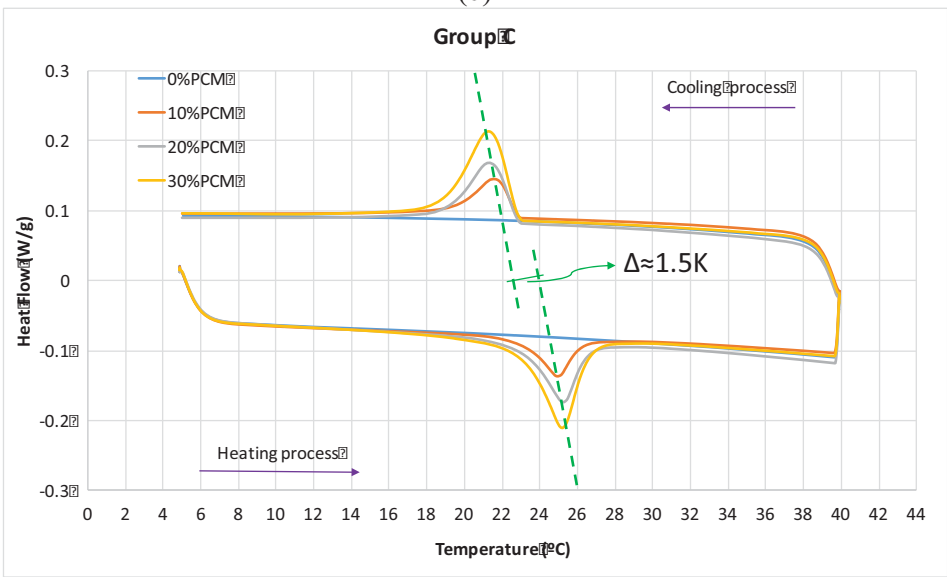
Group C
0%PCM
10%PCM
20%PCM
30%PCM
Cooling process
Δ≈1.5K
Heating process
Heat Flow (W/g)
Temperature (°C)

(c)

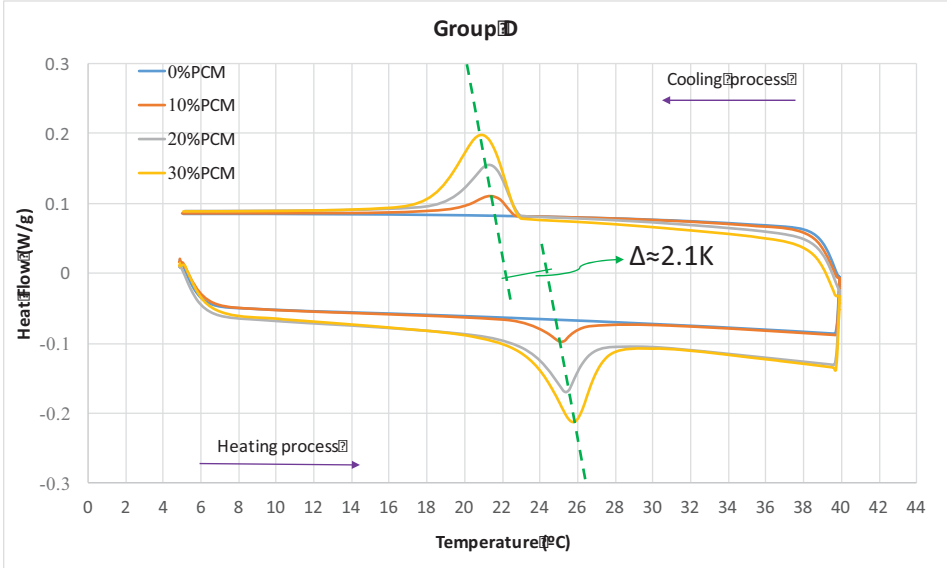
Group D
0%PCM
10%PCM
20%PCM
30%PCM
Cooling process
Δ≈2.1K
Heating process
Heat Flow (W/g)
Temperature (°C)

(d)

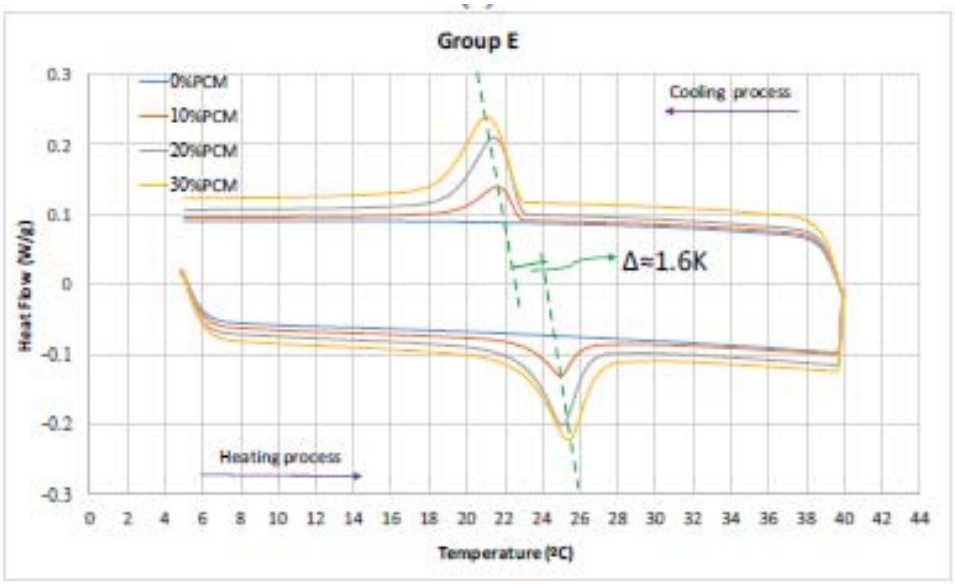

(e)

Fig. (7). DSC curves of the alkali activated mortars with and without PCM upon a cooling and a heating cyclic test with rate of 5°C/min: (a) group A based on 90FA_10CH_12M_2.5S/H_0.8A/B; (b) group B based on 90FA_10CH_12M_2.5S/H_0.7A/B_1.0SP; (c) group C based on 90FA_10CH_12M_2.0S/H_0.7A/B_1.0SP; (d) group D based on 90FA_10CH_12M_1.5S/H_0.7A/B_1.0SP; and (E) group E based on 90FA_10PC_12M_2.5S/H_0.8A/B; Δ stands for the orthogonal distance between peak the two dashed lines.

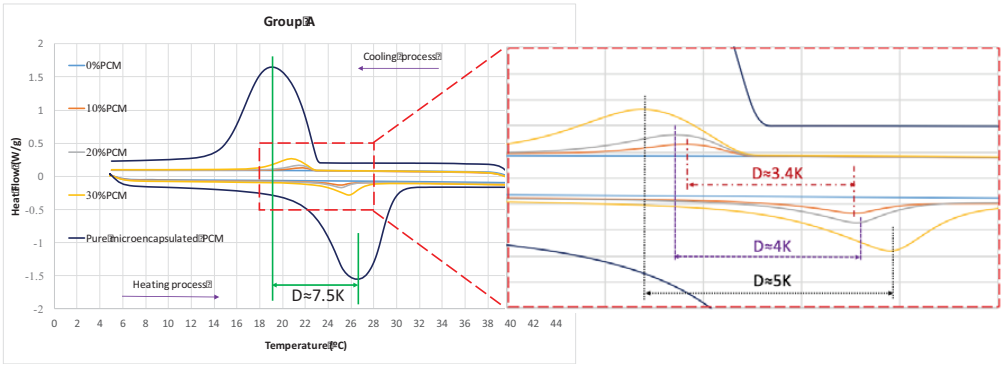

Fig. (8). Comparison between DSC curves for mortars in group A for a heating/cooling cycle at rate of 5 °C/min, highlighting hysteretic behavior of mortars with PCM. “D” stands for the temperature difference between the peaks of heating and cooling processes.

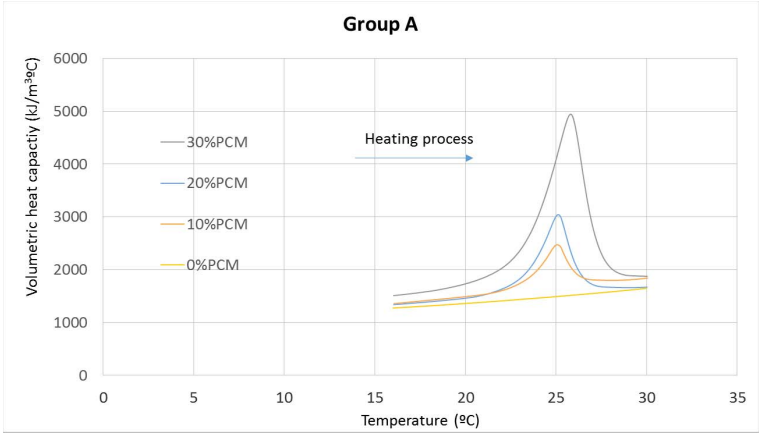

Fig. (9). Results for volumetric specific heat capacities of mortars at group A upon the heating process.

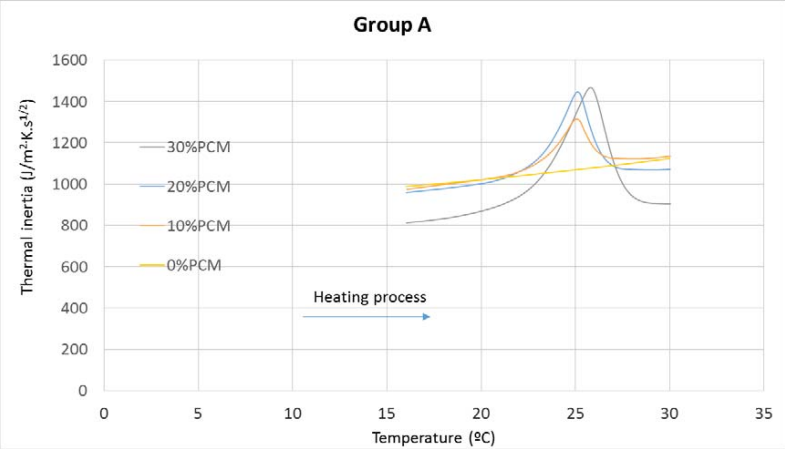

Fig. (10). Thermal inertia of mortars in function of temperature.

$$C_{pv} = C_p \times \rho \tag{1}$$

Where C_p is the specific heat capacity of the material and ρ is the density of the material. Such value ascribes the ability of the material in terms of energy storage in a certain volume while undergoing a given temperature change. The thermal inertia I is calculated according to the following equation [11] with respect to the thermal conductivity of the material λ:

$$I = \sqrt{\rho \times C_p \times \lambda} \tag{2}$$

The high thermal inertia describes a material that is characterized by high thermal mass and high thermal conductivity. In fact, higher thermal inertia means "fastermaterials" that are able to be thermally activated and more thermal load can be stored during the dynamic thermal process. Results in Fig. (**9**) show that the thermal inertia of PCM based mortars is higher than that of the plain mortar (particularly for the phase change range temperature), thus highlighting its higher potential for attenuating the effect of external environment temperatures on buildings [11]. The values of the specific enthalpy are shown in Fig. (**11**) for both heating and cooling processes. It can be observed that the specific enthalpy value is increased systematically for cooling processes regardless of the PCM mortar type. The results show that the specific enthalpies for mortars at different groups from A to E are almost the same regardless of PCM percentage. Even though mixtures with 10% PCM in the group D, with 20% PCM in group E and with 30%PCM in group A have shown lower or higher specific enthalpy than those already obtained for PCM mortars. It is further interesting to investigate whether the specific enthalpy values calculated from DSC experiment can be used to predict the energy performance of PCM mortars. Also, if a proportionality is assumed between latent heat capacity of the PCM mortar and the latent heat capacity of the pure microencapsulated PCM, according to its mass fraction of the PCM, the following formula can be considered:

$$H_T = H_{PCM} \times \frac{W_{PCM}\%}{100} \tag{3}$$

Where H_T is the calculated latent heat for the mortar (J/g), H_{pCM} is the latent heat of the pure microencapsulated PCM, W_{pCM}% is the weight percentage of the PCM in the matrix. Fig. (**12**) shows the measured specific enthalpies of the PCM mortars, together with the expected specific enthalpies of the mortars calculated according to Eq. (3). The numerical extrapolated enthalpy values for all studied PCM mortars are quite close in both heating and cooling processes (with <0.5 J/g differences), except for the mortar with the formulation of 90FA_10CH_30PCM_12M_2.5S/H_0.8A/B within group A, with slightly higher differences between numerical extrapolated enthalpies and measured enthalpies. This indicates the feasibility of the extrapolation procedure for the estimation of the specific enthalpy of the PCM mortars.

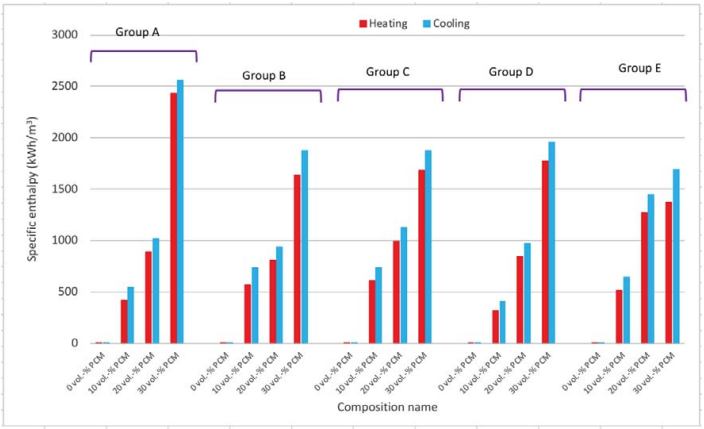

Fig. (11). Specific enthalpy values of the AACB mortars.

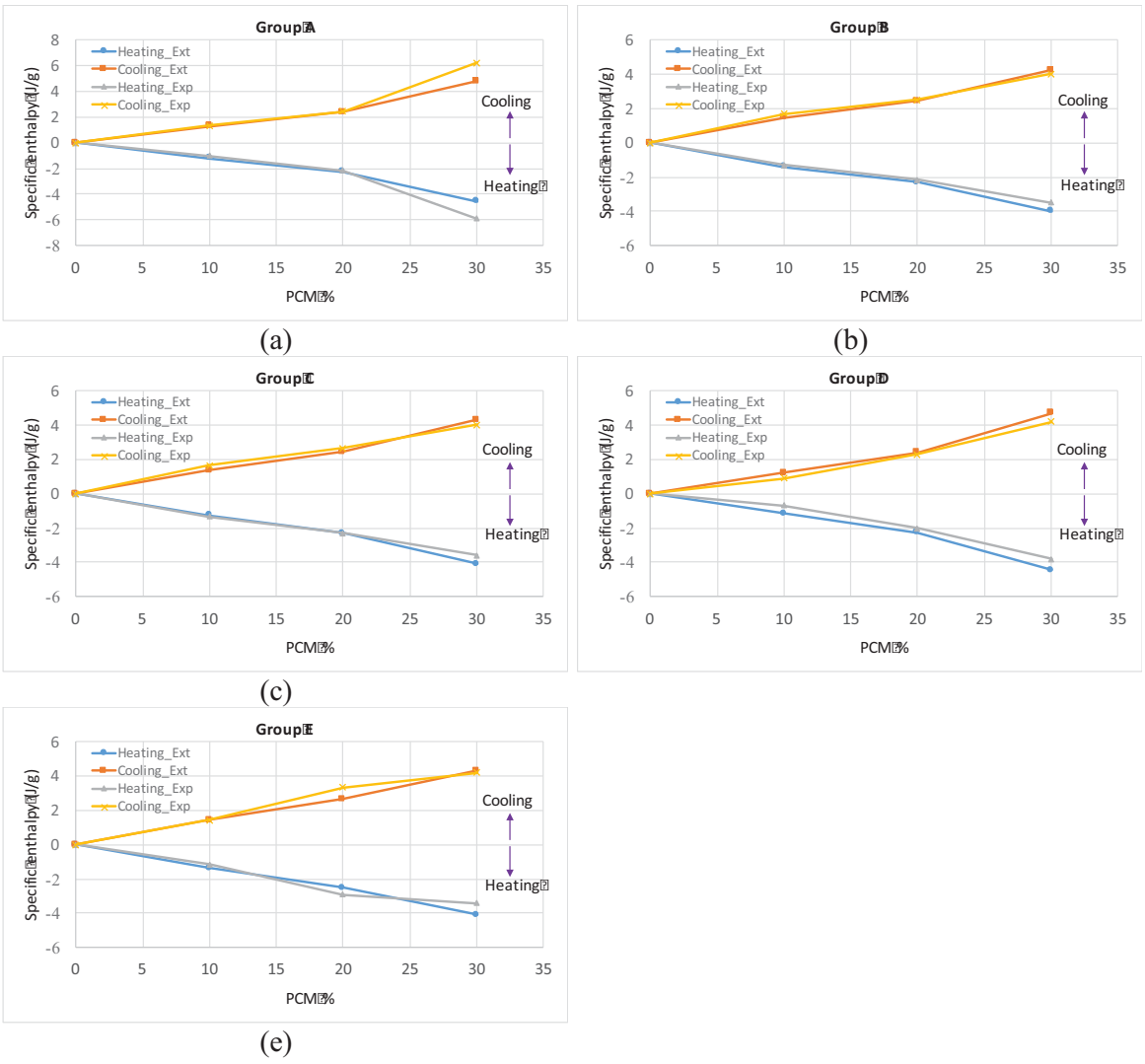

Fig. (12). Heat storage capacity of mortars for different groups: measured values (Exp) and extrapolated values (Ext).

3.1.4. Temperature Monitoring of the Pilot Prototypes

The monitored temperatures for several mixtures within group A under a heating/cooling conditions are shown in Fig. (**13**). It can be observed that the difference of temperature amplitude between the enclosed part (right side) and imposed heating load (left side), for case without PCM was of 3 °C, whereas the cases with 10% PCMs, 20%PCM and 30%PCM were associated to smaller internal temperature difference amplitudes of 3.3 °C, 3.5 °C and 4 °C. These internal temperature differences at laboratory scale are consistent with the concept of improved heat capacity of the PCM mortars which, in turn, is in line with other studies [33]. The time delay between the maximum temperatures registered at the left side and right side for the case with 30% PCM was of nearly 3 min, in opposition to a smaller delay of 2.7 min (for the case with 20% PCM), 2.5 min (for the case with 20% PCM) and smaller delay associated to the case without PCM (1.5 min). It is interesting to note that the achieved temperature variations for different case scenarios with PCM were close to the phase change transition of microencapsulated PCM (Fig. **7**). The results for the cases at group A revealed that PCM acts by reducing inside temperature amplitudes during the heating period, leveling them and turning them closer to melting temperature of the PCM (around 26 °C). It is also worth noticing that the differences in performance were not only caused by the thermal energy storage capacity. Indeed, the PCM mortars had a slightly smaller thermal conductivity that has also contributed to reduce heat fluxes inwards and outwards the panel within prototype. Nonetheless, the PCM-based mortars also had a lower density than the case of mortars without PCM, so its volumetric heat capacity could have been reduced accordingly. In general, during the heating process, for the mortar without PCM, the temperature changeon the right side of the panel depends on the heat capacity of the mortar, whereas for the PCM mortars, the latent heat of the PCMs provides much higher storage and thus shows a lower amplitude. It can be further stated that the incorporation of PCM allows the mortar to delay the temperature change. The overall observations for the mortars at group B to E were similar to those already reported above for mortar at group A. The incorporation of PCM leads to a significant attenuation of the amplitude of the effects of the heating temperature, with a reduction in peak temperatures and time delaying effect. Fig. (**14**) indicates that the mixture 90FA_10PC_30PCM_12M_2.5S/H_0.8A/B from group E with temperature difference of 5.2 °C had the best performance in terms of temperature amplitude and the mortar with the formulation of 90FA_10CH_30PCM_12M_2.5S/H_0.8A/B from group A had shown the worst with 23% less performance (4 °C).

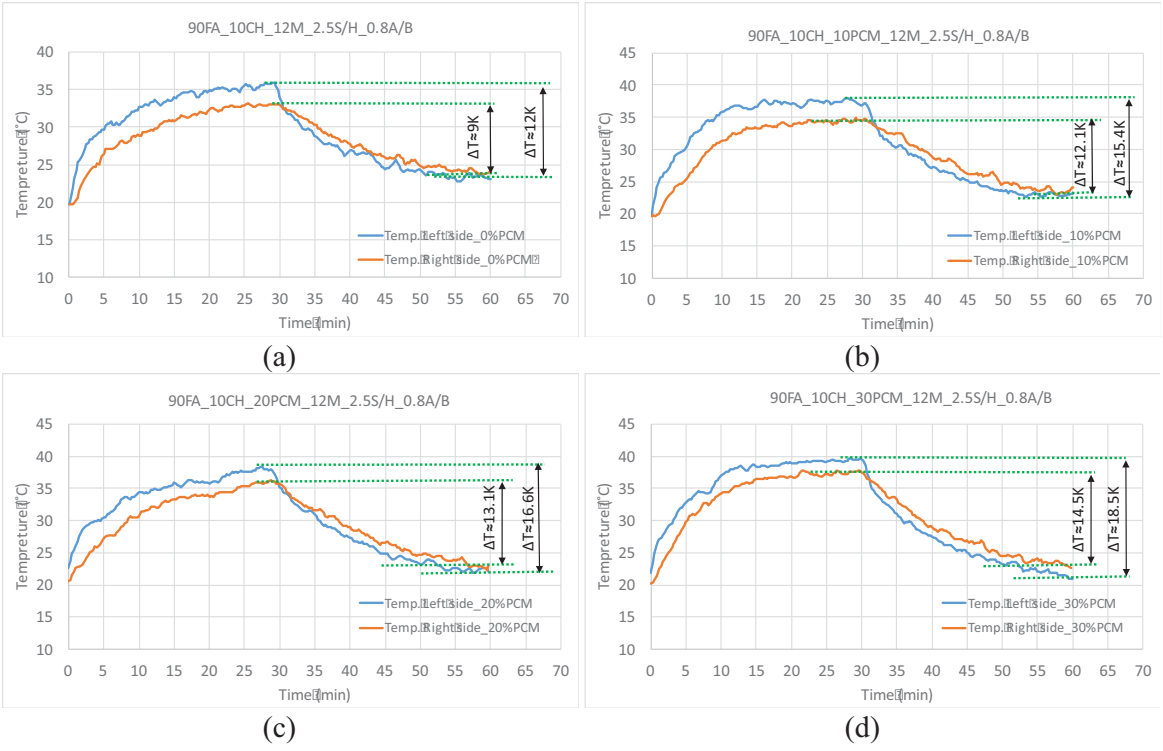

Fig. (13). Indoor temperature variation curves of the pilot prototypes with the interior panel with mortar containing different mass percentages of the microencapsulated PCM at group A: (a) without PCM; (b) 10%PCM; (c) 20%PCM; and (d) 30%PCM.

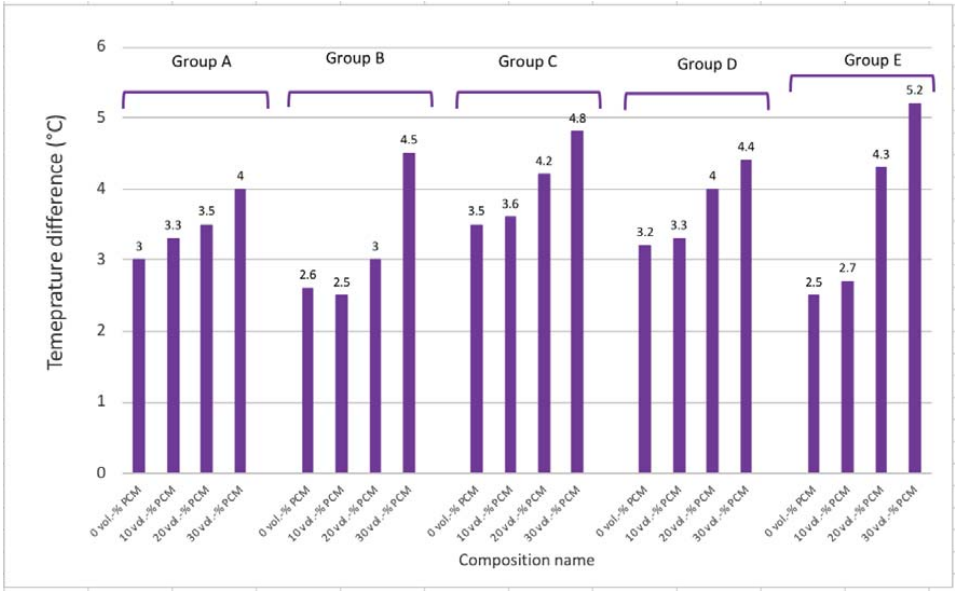

Fig. (14). Temperature differences between the maximum temperature and minimum temperature monitored at left and right side of the panel within prototype along tested time for all compositions.

CONCLUSION

This paper discloses results related to the transient thermal behavior of alkali-activated mortars containing microencapsulated PCM. Firstly, characterization of the materials in the scope of this study was performed. Second, several sets of panels were designed and placed within a laboratory scale prototype to evaluate the capacity of the tested mortars in affecting inner temperatures of the prototypes. Then, five groups with different percentages of PCM incorporations (0%, 10%, 20% and 30%), were submitted to heating temperatures and cooling temperatures and inner air temperature of the prototype was recorded. The following main conclusions can be made. The addition of PCM reduced the density of the mortars.

The thermal conductivity of mortars decreases with the increase in the percentage of the PCM. The main thermal characteristics of the developed mortars were : average specific enthalpies for all the studied groups were ≈1.5 J/g, ≈2.5 J/g and ≈4 J/g for the mortar with 10%PCM, 20%PCM and 30%PCM, respectively, in a melting temperature range from ≈22°C to ≈27°C and solidification temperature range from 19 °C to 23°C. The results of DSC test confirmed that the PCM particles have good compatibility with alkali-activated binder. The thermal performance of PCM mortars showed a strong reduction in the temperature extremes. This situation was monitored in heating and cooling loads.

CONSENT FOR PUBLICATION

Not applicable.

CONFLICT OF INTEREST

The authors declare no conflict of interest, financial or otherwise.

ACKNOWLEDGMENTS

The authors would like to acknowledge the financial support from the Foundation for Science and Technology (FCT) for the frame of research project with Ref. IF/00706/2014-UM.2.15 as well as C-TAC and ISISE research units.

REFERENCES

[1] M. Hook, and X. Tang, "Depletion of fossil fuels and anthropogenic climate change-A review", *Ener. Pol.,* vol. 52, pp. 797-809, 2013. [http://dx.doi.org/10.1016/j.enpol.2012.10.046]

[2] COM (2011) 885/2,Energy Roadmap 2050. European Commission, Brussels https:// ec.europa.eu/energy/ sites/ener/ files/documents/ 2012_energy_roadmap_2050_en_0.pdf

[3] H. Lund, and F. Hvelplund, "The economic crisis and sustainable development: The design of job creation strategies by use of concrete institutional economics", *Energy,* vol. 43, pp. 192-200, 2012.
[http://dx.doi.org/10.1016/j.energy.2012.02.075]

[4] E.P.B.D. Recast, "Energy performance of buildings, European Union", Directive 2010/31/EU of the European Parliament and of the Council of May 19th, on the Official Journal of the European Union; June, 2010. https:// eur-lex.europa.eu/ LexUriServ/ LexUriServ. do?uri=OJ:L:2010:153:0013: 0035:EN:PDF

[5] F. Pacheco-Torgal, "Eco-efficient construction and building materials research under the EU Framework Programme Horizon 2020", *Constr. Build. Mater.,* vol. 51, pp. 151-162, 2014.
[http://dx.doi.org/10.1016/j.conbuildmat.2013.10.058]

[6] K. Kheradmand, J. Castro-Gomes, M. Azenha, P.D. Silva, J.L.B. de Aguiar, and S.E. Zoorob, "Assessing the feasibility of impregnating phase change materials in lightweight aggregate for development of thermal energy storage systems", *Constr. Build. Mater.,* vol. 89, pp. 48-59, 2015.
[http://dx.doi.org/10.1016/j.conbuildmat.2015.04.031]

[7] P. Sukontasukkul, N. Nontiyutsirikul, S. Songpiriyakij, K. Sakai, and P. Chindaprasirt, "Use of phase change material to improve thermal properties of lightweight geopolymer panel", *Mater. Struct.,* vol. 49, pp. 4637-4645, 2016.
[http://dx.doi.org/10.1617/s11527-016-0812-x]

[8] M. Kheradmand, M. Azenha, J.L.B. de Aguiar, and J. Castro-Gomes, "Experimental and numerical studies of hybrid PCM embedded in plastering mortar for enhanced thermal behaviour of buildings", *Ener.,* vol. 94, pp. 250-261, 2016.
[http://dx.doi.org/10.1016/j.energy.2015.10.131]

[9] S. Cunha, J. Aguiar, and F. Pacheco-Torgal, "Effect of temperature on mortars with incorporation of phase change materials", *Constr. Build. Mater.,* vol. 98, pp. 89-101, 2015.
[http://dx.doi.org/10.1016/j.conbuildmat.2015.08.077]

[10] L. Cabeza, C. Castellón, M. Nogués, M. Medrano, R. Leppers, and O. Zubillaga, "Use of microencapsulated PCM in concrete walls for energy savings", *Energy Build.,* vol. 39, pp. 113-119, 2007.
[http://dx.doi.org/10.1016/j.enbuild.2006.03.030]

[11] M. Kheradmand, "Incorporation of hybrid phase change materials in plastering mortars for increased energy efficiency in buildings", [PhD thesis], University of Minho, 2016.

[12] M. Theodoridou, L. Kyriaou, and I. Ioannou, "PCM-enhanced lime plasters for vernacular and contemporary architecture", *Ener. Proc.,* vol. 97, pp. 539-545, 2016.
[http://dx.doi.org/10.1016/j.egypro.2016.10.070]

[13] COM (571) Roadmap to a Resource Efficient Europe, Brussels. http:// www.europarl.europa.eu/ meetdocs/ 2009_2014/ documents/ com/ com_com(2011)0571_/ com_com(2011)0571_ en.pdf

[14] COM 398 final. Towards a circular economy: A zero waste programme for Europe. Communication from the Commission to the European Parliament, the Council, the European Economic and Social Committee and the Committee of the Regions. Brussels, 2.7.2014 https:// eur-lex.europa.eu/ legal-content/ EN/TXT/ ?uri=celex%3A52014DC0398

[15] J.L. Provis, "Geopolymers and other alkali activated materials: why, how, and what?", *Mater. Struct.,* vol. 47, pp. 11-25, 2014.
[http://dx.doi.org/10.1617/s11527-013-0211-5]

[16] C. Ferone, F. Colangelo, F. Messina, L. Santoro, and R. Cioffi, "Recycling of pre-washed municipal solid waste incinerator fly ash in the manufacturing of low temperature setting geopolymer materials", *Materials (Basel),* vol. 6, no. 8, pp. 3420-3437, 2013.
[http://dx.doi.org/10.3390/ma6083420] [PMID: 28811443]

[17] J. Payá, J. Monzó, M.V. Borrachero, and M.M. Tashima, "Reuse of aluminosilicate industrial waste materials in the production of alkali-activated concrete binders", In: Handbook of Alkali-Activated Cements, Mortars and Concretes", F.Pacheco-Torgal, J. Labrincha, A.Palomo, C. Leonelli, P. Chindaprasirt, Eds. Cambridge: WoodHead Publishing, 2014, pp.487-518.

[18] P. Chindaprasirt, and T. Cao, "Reuse of recycled aggregate in the production of alkali-activated concrete", Handbook of Alkali-Activated Cements, Mortars and Concretes", F.Pacheco-Torgal, J. Labrincha, A.Palomo, C. Leonelli, P. Chindaprasirt, Eds. Cambridge: WoodHead Publishing, 2014, pp.519-538.

[19] K. Tzanakos, A. Mimilidou, K. Anastasiadou, A. Stratakis, and E. Gidarakos, "Solidification/stabilization of ash from medical waste incineration into geopolymers", *Waste Manag.,* vol. 34, no. 10, pp. 1823-1828, 2014.
[http://dx.doi.org/10.1016/j.wasman.2014.03.021] [PMID: 24785364]

[20] S. Bernal, E. Rodríguez, A. Kirchheim, and J. Provis, "Management and valorisation of wastes through use in producing alkali-activated cement materials", *J. Chem. Technol. Biotechnol.,* vol. 91, pp. 2365-2388, 2016.
[http://dx.doi.org/10.1002/jctb.4927]

[21] F. Pacheco-Torgal, Z. Abdollahnejad, S. Miraldo, and M. Kheradmand, "Alkali-activated cement-based binders (AACB) as durable and cost competitive low CO2 binders: Some shortcomings that need to be adressed", In: Handbook of low carbon concrete, Nazari & Sanjayan Eds, Waltham, Elsevier Science and Tech, 2017, pp.195-216.

[22] American Coal Ash Association. 2016. https:// www.acaa-usa.org/ Publications/

[23] ASTM C618 - 15, Standard Specification for Coal Fly Ash and Raw or Calcined Natural Pozzolan for Use in Concrete, ASTM International, West Conshohocken, PA, https:// www.astm.org

[24] B. EN, 1015-10: Methods of test for mortar for masonry. Determination of dry bulk density of hardened mortar, (1999).

[25] ISO:8301, Thermal insulation: determination of steady state thermal resistance and related properties, heat flow meter apparatus, 1991.

[26] T. Lecompte, P. Le Bideau, P. Glouannec, D. Nortershauser, and S. Le Masson, "Mechanical and thermo-physical behaviour of concretes and mortars containing phase change material", *Energy Build.,* vol. 94, pp. 52-60, 2015. [http://dx.doi.org/10.1016/j.enbuild.2015.02.044]

[27] M. Kheradmand, M. Azenha, J.L.B. de Aguiar, and K.J. Krakowiak, "Thermal behavior of cement based plastering mortar containing hybrid microencapsulated phase change materials", *Energy Build.,* vol. 84, pp. 526-536, 2014. [http://dx.doi.org/10.1016/j.enbuild.2014.08.010]

[28] H. Zhang, F. Xing, H-Z. Cui, D-Z. Chen, X. Ouyang, S-Z. Xu, J-X. Wang, Y-T. Huang, J-D. Zuo, and J-N. Tang, "A novel phase-change cement composite for thermal energy storage: Fabrication, thermal and mechanical properties", *Appl. Energy,* vol. 170, pp. 130-139, 2016. [http://dx.doi.org/10.1016/j.apenergy.2016.02.091]

[29] L. Haurie, S. Serrano, M. Bosch, A.I. Fernandez, and L.F. Cabeza, "Single layer mortars with microencapsulated PCM: Study of physical and thermal properties, and fire behaviour", *Energy Build.,* vol. 111, pp. 393-400, 2016. [http://dx.doi.org/10.1016/j.enbuild.2015.11.028]

[30] Z. Zhang, G. Shi, S. Wang, X. Fang, and X. Liu, "Thermal energy storage cement mortar containing n-octadecane/expanded graphite composite phase change material", *Renew. Energy,* vol. 50, pp. 670-675, 2013. [http://dx.doi.org/10.1016/j.renene.2012.08.024]

[31] C. Castellón, E. Günther, H. Mehling, S. Hiebler, and L.F. Cabeza, "Determination of the enthalpy of PCM as a function of temperature using a heat□flux DSC-A study of different measurement procedures and their accuracy", *Int. J. Energy Res.,* vol. 32, pp. 1258-1265, 2008. [http://dx.doi.org/10.1002/er.1443]

[32] C. Castellón, E. Günther, H. Mehling, S. Hiebler, and L.F. Cabeza, "Determination of the enthalpy of PCM as a function of temperature using a heat□flux DSC-A study of different measurement procedures and their accuracy", *Int. J. Energy Res.,* vol. 32, pp. 1258-1265, 2008. [http://dx.doi.org/10.1002/er.1443]

[33] R. Ye, X. Fang, Z. Zhang, and X. Gao, "Preparation, Mechanical and Thermal Properties of Cement Board with Expanded Perlite Based Composite Phase Change Material for Improving Buildings Thermal Behavior", *Materials (Basel),* vol. 8, no. 11, pp. 7702-7713, 2015. [http://dx.doi.org/10.3390/ma8115408] [PMID: 28793671]